SMC-TR-92-44

AEROSPACE REPORT NO.
TR-92(2935)-3

Surface Analyses of Composites Exposed to the Space Environment on LDEF

Prepared by

J. J. MALLON, J. C. UHT, and C. S. HEMMINGER
Mechanics and Materials Technology Center
Technology Operations

31 August 1992

Prepared for

SPACE AND MISSILE SYSTEMS CENTER
AIR FORCE MATERIEL COMMAND
Los Angeles Air Force Base
P. O. Box 92960
Los Angeles, CA 90009-2960

Engineering and Technology Group

THE AEROSPACE CORPORATION
El Segundo, California

This report was submitted by The Aerospace Corporation, El Segundo, CA 90245, under Contract No. F04701-88-C-0089 with the Space Systems Division, P.O. Box 92960, Los Angeles, CA 90009-2960. It was reviewed and approved for The Aerospace Corporation by R. W. Fillers, Principal Director, Mechanics and Materials Technology Center. Paul Propp was the project officer.

This report has been reviewed by the Public Affairs Office (PAS) and is releasable to the National Technical Information Service (NTIS). At NTIS, it will be available to the general public, including foreign nationals.

This technical report has been reviewed and is approved for publication. Publication of this report does not constitute Air Force approval of the report's findings or conclusions. It is published only for the exchange and stimulation of ideas.

QUANG BUI, Lt, USAF
MOIE Program Manager

PAUL M. PROPP
Wright Lab West Coast Office

UNCLASSIFIED

SECURITY CLASSIFICATION OF THIS PAGE

REPORT DOCUMENTATION PAGE

1a. REPORT SECURITY CLASSIFICATION Unclassified	1b. RESTRICTIVE MARKINGS
2a. SECURITY CLASSIFICATION AUTHORITY	3. DISTRIBUTION/AVAILABILITY OF REPORT Approved for public release; distribution unlimited
2b. DECLASSIFICATION/DOWNGRADING SCHEDULE	
4. PERFORMING ORGANIZATION REPORT NUMBER(S) TR-92(2935)-3	5. MONITORING ORGANIZATION REPORT NUMBER(S) SMC-TR-92-44
6a. NAME OF PERFORMING ORGANIZATION The Aerospace Corporation Technology Operations 6b. OFFICE SYMBOL *(If applicable)*	7a. NAME OF MONITORING ORGANIZATION Space and Missile Systems Center
6c. ADDRESS *(City, State, and ZIP Code)* El Segundo, CA 90245-4691	7b. ADDRESS *(City, State, and ZIP Code)* Los Angeles Air Force Base Los Angeles, CA 90009-2960
8a. NAME OF FUNDING/SPONSORING ORGANIZATION 8b. OFFICE SYMBOL *(If applicable)*	9. PROCUREMENT INSTRUMENT IDENTIFICATION NUMBER F04701-88-C-0089
8c. ADDRESS *(City, State, and ZIP Code)*	10. SOURCE OF FUNDING NUMBERS PROGRAM ELEMENT NO. / PROJECT NO. / TASK NO. / WORK UNIT ACCESSION NO.

11. TITLE *(Include Security Classification)*

Surface Analyses of Composites Exposed to the Space Environment on LDEF

12. PERSONAL AUTHOR(S)

Mallon, Joseph J.; Uht, Joseph C.; and Hemminger, Carol S.

13a. TYPE OF REPORT	13b. TIME COVERED	14. DATE OF REPORT *(Year, Month, Day)*	15. PAGE COUNT
	FROM _____ TO _____	1992 August 31	30

16. SUPPLEMENTARY NOTATION

17. COSATI CODES			18. SUBJECT TERMS *(Continue on reverse if necessary and identify by block number)*
FIELD	GROUP	SUB-GROUP	Satellite contamination

19. ABSTRACT *(Continue on reverse if necessary and identify by block number)*

We have conducted a series of surface analyses on carbon fiber/polyarylacetylene matrix composites that were exposed to the space environment on the Long Duration Exposure Facility (LDEF) satellite. These composite panels were arranged in pairs on both the leading edge and trailing edge of LDEF. None of the composites were catastrophically damaged by nearly six years of exposure to the space environment. Composites on the leading edge exhibited 5 mils of surface erosion, but trailing edge panels exhibited no physical appearance changes due to exposure.

Scanning electron microscopy (SEM) was used to show that the erosion morphology on the leading edge samples was dominated by crevasses parallel to the fibers with triangular cross sections 10 to 100 μm in depth. The edges of the crevasses were well defined and penetrated through both matrix and fiber. The data suggest that the carbon fibers are playing a significant role in crevasse initiation and/or enlargement, and in the overall erosion rate of the composite. X-ray photoelectron spectroscopy (XPS) and energy dispersive x-ray spectroscopy (EDS) results showed the presence of silicone and hydrocarbon contamination from in-flight sources. The role of contamination in crevasse initiation and enlargement is unknown as this time.

20. DISTRIBUTION/AVAILABILITY OF ABSTRACT	21. ABSTRACT SECURITY CLASSIFICATION
[X] UNCLASSIFIED/UNLIMITED [ ] SAME AS RPT. [ ] DTIC USERS	Unclassified
22a. NAME OF RESPONSIBLE INDIVIDUAL	22b. TELEPHONE *(Include Area Code)* / 22c. OFFICE SYMBOL

DD FORM 1473, 84 MAR — 83 APR edition may be used until exhausted. All other editions are obsolete

SECURITY CLASSIFICATION OF THIS PAGE

UNCLASSIFIED

19. ABSTRACT *(Continued)*

These LDEF results demonstrate that the prediction of long term atomic oxygen erosion morphology for composite materials from erosion data obtained on short Space Shuttle missions is difficult. A better understanding of other factors such as thermal cycling and UV exposure, which may influence erosion, is necessary to improve the accuracy of the predictions.

PREFACE

This experiment was initially conceived by Dr. James Gee, Camille Gaulin, and Clark Williams. The LDEF deintegration effort was performed by Sandra Gyetvay, Laana Fishman, and Dr. Michael Meshishnek with funding from the Space Test Program (administered by the Air Force SSD/CLP). The initial examination and photography of the composite samples were performed by Sandra Gyetvay, Laana Fishman, and Dr. Michael Meshishnek with funding from SDIO/TNK under the Space Environment Effects (SEE) Program, administered by Wright Laboratory Materials Directorate. The authors would like to credit Mr. Ca Su with the preparation of the cross-section samples. We would also like to thank Dr. Sherrie Zacharius, Dr. Howard Katzman, Dr. Gary Steckel, Dr. Gerald Rellick, and Dr. Wayne Stuckey for helpful suggestions and comments. This work was supported by the Wright Laboratory Materials Directorate and by The Aerospace Corporation Mission Oriented Investigation and Experimentation program.

CONTENTS

FIGURES

TABLES

I. INTRODUCTION

The Long Duration Exposure Facility (LDEF) was an unmanned satellite that was placed into low Earth orbit (LEO) by the Space Shuttle Challenger on April 7, 1984 and retrieved by the Space Shuttle Columbia on January 12, 1990. One of the purposes of the LDEF experiment was to determine the effect of the space environment on various materials and devices. Fifty-seven science and technology experiments were included on LDEF. The experiments were organized into four categories: (1) materials, coatings, and thermal systems; (2) power and propulsion; (3) science; and (4) electronics and optics. The original LDEF mission was planned to be about one year in length, but the Challenger disaster and subsequent recovery effort resulted in a mission of nearly six years (about 32,400 orbits). Since most satellites are destroyed as they reenter the atmosphere, very little data exist on the long-term effect of the space environment on spacecraft. There are currently no firm plans to place another LDEF into orbit, so the information that is extracted from this LDEF will probably constitute the bulk of the data base for a generation of spacecraft design engineers.

LDEF consisted of a 12-sided aluminum framework cylinder, 9.1 m long and 4.3 m in diameter, to which experiment trays were attached. While in orbit, LDEF was stabilized about all three axes as shown in Figure 1a. One end was always pointed toward the Earth, the other end always pointed toward space; one side, known as the leading edge, continually faced into the velocity vector. The side 180° from the leading edge is known as the trailing edge. LDEF was initially placed into a nearly circular orbit with an altitude of 480 km and an inclination of 28.5°. By the end of the mission, it was at an altitude of only 310 km due to atmospheric drag. Many of the experiments on LDEF were arranged in pairs, with one-half of the pair on the leading edge and one-half on the trailing edge. The exposure of the experiments to atomic oxygen and solar radiation was a function of position on the satellite. By the end of the mission, experiments on the leading edge had been exposed to an atomic oxygen fluence estimated at 8.3×10^{21} atoms/cm^2, those on the trailing edge to 3.3×10^3 atoms/cm^2. The level of radiation exposure also ranged from about 6500 equivalent sun hours to about 11,100 equivalent sun hours, depending on position.

Experiment M0003, Space Environment Effects on Materials, consisted of 19 subexperiments and was flown as part of the materials, coatings, and thermal systems experimental category. The overall objective of this experiment was to obtain data concerning structure and property changes in materials that had been exposed to the space environment and to understand the reasons for these changes. Subexperiment MOOO3-16, Advanced Composite Materials, included three pairs of carbon fiber composite panels. Each pair consisted of a leading edge panel and a trailing edge panel. The leading edge panels were located on Bay D of Row 9 (see Figure 1b) and the trailing edge panels were located on Bay D of Row 3. Row 9 received about 8.3×10^{21} atoms/cm^2 of atomic oxygen fluence and 11,100 equivalent sun hours of radiation exposure; the corresponding values for the Row 3 are 3.7×10^3 atoms/cm^2 and 11,100 equivalent sun hours, respectively. The difference in atomic oxygen exposure between Row 9 and Row 3 was more than 18 orders of magnitude, but there was essentially no difference in radiation exposure.

The three composites selected for the experiment were carbon/poly(arylacetylene) materials that were under development at The Aerospace Corporation in 1984 as replacements for more traditional composites such as carbon/epoxy. Poly(arylacetylene) (PAA) is a hydrophobic matrix made by the polycyclotrimerization reaction of m-diethynylbenzene (DEB).[1-4] The cyclotrimerization of DEB is shown in Figure 2. Further cyclotrimerization of available ethynyl groups results in products with increasing molecular weight. The reaction is typically halted (by cooling the reaction mixture) when the toluene solution reaches the desired viscosity; precipitation of the polymer eventually occurs if the reaction is allowed to proceed further. One of the PAA composites (panel C) contained an additional component, poly(phenylquinoxiline) (PPQ), which was added to increase the toughness of the PAA matrix.

Composites are principally used in space as structural components, so the effect of the space environment on the mechanical and physical properties of the composites flown on LDEF is of great interest to the design community. In an effort to extract the maximum possible amount of information from these one-of-a-kind samples, our initial attention has been focused on an extensive series of nondestructive surface analyses. Much can be learned about the effect of the space environment (particularly atomic oxygen) on materials and the nature of the contamination environment from surface analyses. The presence of even small amounts of contamination on thermal control surfaces and optical systems can be very detrimental to their operation. In this document we will report on the surface analyses of carbon/PAA composite samples as determined by optical microscopy, scanning electron microscopy (SEM), energy dispersive x-ray (EDS) spectroscopy, and x-ray photoelectron spectroscopy (XPS).

II. EXPERIMENTAL

The identities of the composite panels are shown in Table 1. Each panel was about 1.5 in. x 3.5 in. x 0.13 in. in size. Poly(arylacetylene) (PAA) was prepared in toluene solution from diethynylbenzene and 1,4-diphenylbutadiyne in a manner analogous to that of Jabloner.[1] HA-43 is a commercial version of PAA that was supplied by Hercules, Inc. Poly(phenylquinoxiline) was prepared in m-cresol by the condensation reaction of bis-benzil and 3,3',4,4'-tetraamin- obiphenyl (see Reference 5 for details). T300 fabric was purchased from Ferro Corp. The fabric was impregnated with a toluene solution of the resin, then allowed to air dry to evaporate the solvent. The composite panels A, B, and C were molded as follows:

A. HA-43/T300: Thirteen prepreg plies of HA-43/T300 were laid up and molded in a press at 500 psi and 177°C for three hours, then allowed to cool to room temperature. The resin content of the resulting panel was about 37% by weight.

B. PAA/T300: T300 fabric was impregnated with a toluene solution of PAA resin and the solvent was allowed to evaporate in air. Thirteen plies of the resulting prepreg were laid up and cured in a press at 500 psi and 177°C for three hours, then allowed to cool to room temperature. The resin content of the resulting panel was about 22% by weight.

C. HA-43, PPQ blend/T300: A resin mixture consisting of 86g of dry HA-43, 86g of dry PPQ, 2300g of chloroform, 207g of 1,1,1-trichloroethane, and 22g of m-cresol was prepared. T300 fabric was impregnated with this resin and the solvent was allowed to evaporate in air. Thirteen plies of the resulting prepreg were laid up and cured in a press at 1000 psi and 250°C for six hours, then allowed to cool to room temperature. The resin content of the resulting panel was about 33% by weight.

A. SCANNING ELECTRON MICROSCOPY/ENERGY DISPERSIVE X-RAY SPECTROSCOPY (SEM/EDS)

Analyses were performed on the front and back surfaces of the three pairs of composites. Each sample was studied as received, with no sample preparation being necessary except pumpdown at high vacuum for about 24 hours before introduction to the SEM (due to the large size of these samples). A JEOL 840 SEM with an EDAX 9900 EDS system was used for this study. Electron micrographs were acquired using accelerating voltages ranging from 5kV to 25kV. EDS data were acquired using an accelerating voltage of 15kV, which allowed for the acquisition of the lower atomic number elements, such as carbon and oxygen, while still exciting x-ray fluorescence from heavier elements.

B. X-RAY PHOTOELECTRON SPECTROSCOPY (XPS)

Preparation for surface analysis by XPS involved cutting a segment approximately 1/2 in. x 1/2 in. from one end of each composite panel. This was necessary because the original panels were too large to be accommodated by the VG ESCALAB MKII used for the analyses. A dry cut

Table 1. Composition and Sample Number of LDEF Composite Panels

NASA Sample No.	Abbreviated Sample ID	Sample Composition (Resin/Fiber)
L3-IV-16-72A	L-A	HA-43/T300
T3-IV-16-87A	T-A	HA-43/T300
L3-IV-16-73B	L-B	PAA/T300
T3-IV-16-88B	T-B	PAA/T300
L3-IV-16-74C	L-C	HA-43, PPQ blend/T300
T3-IV-16-89C	T-C	HA-43, PPQ blend/T300

of the samples minimized surface contamination from the sample preparation step. Each sample was mounted on top of a VG "powder stub" using four Ta foil tabs that were spot welded around the stub periphery. During analysis of each exposed surface, the backside was in contact only with the top rim of the powder stub, a 1/2 in. diameter circle. This minimized surface contact contamination of the backsides, so that each sample could be flipped over and remounted for the comparative analysis of the backside.

The Al Kα source was chosen for x-ray irradiation. Survey scans from 0 to 1100 eV binding energy were acquired to qualitatively determine the sample surface composition. High resolution elemental scans were subsequently run to obtain semiquantitative elemental analyses from peak area measurements and chemical state information from the details of binding energy and shape. Measured peak areas for all detected elements were corrected by elemental sensitivity factors before normalization to give surface mole %. The quantitation error on a relative basis is ≤10% for components >1 mole %. Large uncertainties in the relative elemental sensitivity factors can introduce absolute errors of a factor of 2 or even greater. All elements of the periodic table except H and He can be detected by XPS. The detection limit is about 0.1 surface mole %, but spectral overlaps between large peaks and small peaks can make it impossible to detect minor components. Scanning electron beam imaging was used to set up the sample surface analysis area in most cases. Imaging allowed a more accurate avoidance of the sample edge areas, which were masked from line-of-sight exposure to the space environment by the mounting hardware.

C. OPTICAL MICROSCOPY

After examination by XPS, the cut samples were embedded in epoxy, cut, and polished so that the cross section of the sample could be examined by both optical microscopy and SEM.

III. RESULTS AND DISCUSSION

The composition and sample number (assigned by NASA according to position on LDEF) of each of the composite panels on LDEF is shown in Table 1. Table 1 also shows abbreviated ID numbers, which will be used throughout this discussion. The prefixes "L" and "T" refer to either a leading or trailing edge location, respectively, on LDEF (see Figure 1). The side of the panel that was subjected to the space environment will be referred to as the "exposed" face and the reverse side of the panel, which was mounted flat against LDEF, will be referred to as the "backside". The backside of each panel functions as a convenient control for the exposed side since laboratory control samples were not available. On-orbit photography of the composite samples by the crew of the Space Shuttle Columbia showed that the samples were intact and relatively undamaged. After examination and photography at Kennedy Space Center, the experiment trays were flown to Aerospace and deintegrated by Aerospace personnel. Deintegration and the initial, cursory examination of individual samples was performed in a class 10,000 clean room. The samples were then packaged into individual, closed boxes for storage between experiments.

A. MICROSCOPY

The initial visual and light microscopy examinations of the samples showed that none of the composites had been catastrophically damaged by nearly six years of exposure to the space environment. The effect of the large difference in atomic oxygen exposure between the leading and trailing edges, discussed in the introduction, is illustrated in Figure 3, which shows SEM micrographs of L-A and T-A. In both of the micrographs, the right-hand side of the sample was masked from the effects of the space environment by the mounting hardware and shows the pre-flight condition of the sample.

Figure 3 demonstrates that the matrix at the surface has been removed by atomic oxygen. A conductive coating is usually applied to composites before SEM examination because the polymeric resin at the surface is nonconductive. The quality of SEM images obtained from uncoated composite samples is generally poor because of surface charging. In this study, the degree of surface charging provides a qualitative measure of matrix erosion because the underlying carbon fibers are electrically conductive. In each case, we found that the exposed area of leading edge samples had little or no surface charging, indicating that the conductive carbon fibers were exposed. The trailing edge samples had extensive surface charging and were difficult to image because the nonconductive matrix had not been removed by erosion. In Figure 3, the lack of surface charging on the exposed area of L-A relative to the masked area and relative to T-A in the SEM chamber demonstrates that the nonconductive matrix at the surface of the leading edge samples was removed by atomic oxygen erosion.

On the basis of the cross-sectioned samples discussed in subsequent paragraphs, it is estimated that the erosion of the samples on the leading edge was about 5 mils. For comparison,[6] a reactive polymer such as Kapton or Mylar was eroded to a depth of about 8.8 mils by the atomic oxygen fluence received on Row 9. We hypothesize that the decreased erosion of the composite relative to polymers is probably best understood in terms of a two-step erosion

process. In the first step, the outer layer of organic matrix was removed at roughly the same rate as the other reactive polymers. In the second step, when the carbon fibers became exposed, a lower reaction efficiency for the fibers led to a lower overall (bulk) erosion rate. We have assumed that the PAA matrix is no more resistant to erosion than other polymers, although this assumption may be questionable (see below).

The erosion process results in a morphology on the leading edge samples that is best understood by examining both the SEM microgaphs of the surface and of the cross-sectioned samples. Figure 4 is a 100X SEM micrograph of the same area of L-A as shown in Figure 3a, showing details of the exposed area and of the masked area. The masked area was shielded from the effects of the space environment by the mounting hardware and shows the undamaged state of the composite before flight. Figure 5 is a similar 200X SEM micrograph of L-C showing exposed and masked areas. The exposed surface is characterized by large crevasses that have developed predominantly parallel to the long axis of the fibers. However, the surface SEM micrograph does not clearly elucidate the condition of the remaining exposed fibers. The cross section of the L-A surface shown in Figure 6 dramatically highlights the "peak and valley" morphology associated with crevasse development on the exposed surface. Note that crevasses parallel to the cut of the cross section will not typically be seen. The area shown on the left side of the optical micrograph was masked and shows the relatively smooth preflight condition of the surface. Cross-section optical micrographs of the L-B and L-C samples, shown in Figures 7 and 8, show similar features to the micrograph of L-A. Sharp crevasses, predominantly parallel to the fibers, are also present on these surfaces, suggesting that the crevasse morphology is a general characteristic of the erosion process for this type of composite.

Higher magnification micrographs of the L-A, L-B, and L-C cross sections are shown in Figures 9-14. At this point it may be useful to distinguish between "cracks" and "crevasses". For our purposes, cracks were formed when two previously united sections of the composite became separated. There is no net loss of material during crack formation. The cracks were probably caused by thermal stresses during molding or during flight. In contrast, crevasses were formed when a section of the material, characterized by a sharp triangular cross section, was removed from the surface of the composite. The crevasses are completely absent on trailing edge sample surfaces, suggesting that they develop as a result of atomic oxygen erosion. Figure 13 shows a cross section of L-C, which contains both a surface crack and surface crevasses. The crack is narrow, uniform in width and longer in length than the wider, triangular crevasses. Note that the intersection of the crack with the surface did not cause a crevasse to form; in general, we found no correlation between the location of cracks and crevasses. There is no indication that the crevasses were initiated by surface cracks.

After examining a number of micrographs, we found that the leading edge samples had a number of features in common. All three of the samples, regardless of the matrix composition or fabrication details, exhibited a surface morphology dominated by crevasses with sharp triangular cross sections that ranged from 10 μm to 100 μm in depth. SEM examination of the surface shows that the crevasse direction was strongly correlated with the fiber direction. The majority of the crevasses developed parallel to the long fiber axis. The crevasses traversed both fibers and matrix, and most appeared to have relatively steep sides that met at a well-defined tip. No preferential removal of the matrix relative to the fibers (undercutting) was apparent along the

sides of the crevasse. Although the samples did contain macroscopic cracks, the cracks were not correlated with the crevasses and did not appear to initiate the formation of the crevasses.

The addition of PPQ to the HA-43 matrix of composite C did not have an obvious effect on the erosion rate or pattern of erosion for L-C relative to L-A. L-B, however, was eroded to a lesser degree than the other two composites, as seen by comparing Figure 7 to Figures 6 and 8. Composite B was fabricated using PAA prepared in our laboratory, and also had the lowest resin content. Examination of L-B at high magnification reveals well-defined crevasses comparable to those on L-A and L-C in appearance, but on average significantly less enlarged. With so few samples, it can only be noted at this point that resin content and/or the details of resin composition/fabrication may play an important role in the overall composite erosion rate.

At the present time, we are unable to suggest a mechanism for the formation of the crevasses. Note that many of the crevasses penetrate *into* the fibers! On a microscopic level, no preferential removal of the matrix relative to the fibers was apparent during crevasse enlargement, an observation that seems to contradict our earlier assumption that the PAA matrix eroded faster than the fibers. For instance, the tip of the crevasse shown penetrating into the fiber in Figure 6 is quite sharp. Atomic oxygen exposure of epoxy-embedded fibers on STS-8 resulted in much faster removal of epoxy from between the fibers than erosion of the fibers themselves.[7] Nothing observed on the STS-8 samples led to a prediction that atomic oxygen erosion of the composite surfaces would cause such highly defined crevasses. From STS-8 results, we would have predicted an erosion process that preferentially removed matrix and that would be blunted by the fiber, instead of penetrating so easily. There is no evidence that atomic oxygen scattering has rounded the sides of the crevasse in matrix-rich areas. However, on a macroscopic level, SEM examination of the surface shows a definite pattern that is correlated with the fiber direction. This indicates that the carbon fibers are playing a crucial role in crevasse initiation and/or enlargement. If there were no differences in rate or mechanism between the atomic oxygen erosion of fibers and matrix, a more uniform erosion pattern would be predicted, such as observed for Kapton, Teflon,[8] or graphite.[7] The observed difference in erosion extent on L-B relative to L-A and L-C also suggests that the fibers are limiting the erosion rate. The role of preflight and in-flight contamination in crevasse initiation and enlargement is unknown at this time.

It seems clear from these results that it is very difficult to predict the erosion morphology of composites from information obtained on relatively short STS missions. LDEF was subjected to thousands of thermal cycles, much higher levels of UV radiation, and a much higher atomic oxygen fluence than the samples that were exposed on STS-8. The relative importance of each of these factors and combinations thereof is presently unknown.

B. ENERGY DISPERSIVE X-RAY SPECTROSCOPY (EDS)

At 15kV, x-ray information for EDS surface composition determination comes from a depth of $\leq 1\mu m$. The EDS data show that all of the composites flown on LDEF are contaminated with Si and O. Low levels of Cl and Cu were also present on most of the analyzed samples. Other minor contaminants detected on one or more surfaces included Ca, Al, S, P, Mg, Ni, Fe, and Ti. In each case, the O concentration was higher on the exposed face than on the backside face, and higher on the leading edge exposed surface than on the trailing edge exposed surface, as seen in

Figure 15. EDS data are not readily quantified for the low atomic number elements such as C and O. Therefore, comparison of relative surface concentrations have been approximated for these composite samples by using elemental peak heights (arbitrary units) after setting all of the carbon peaks to the same height. This should be a valid approximation as long as carbon from the fibers and organic matrix gives the major signal in the volume analyzed. It is seen in Figure 16 that the silicon concentration was significantly higher on the leading edge exposed surfaces than on the trailing edge exposed surfaces, or any of the backside surfaces. The exposed leading edge surface of sample B had higher silicon and oxygen concentrations than the exposed leading edge surfaces of samples A and C, which is consistent with the lower extent of erosion on B observed in the micrographs.

C. X-RAY PHOTOELECTRON SPECTROSCOPY

The XPS surface composition results are tabulated in Table 2. The "Imaged?" column in the table indicates whether or not scanning electron beam imaging was used to set up the sample surface analysis area. The experimental depth of analysis is about 50 to 100 Å. Since this depth is roughly 1% of the depth probed by EDS analysis, XPS is much more sensitive to surface contaminants and less sensitive to bulk compositional differences. Examination of the data in Table 2 shows that the surface composition of the fiber/organic matrix composites is complex. Without laboratory controls, the sample backside surfaces serve as flight controls for the exposed surfaces. For five of the six samples the exposed vs backside surface comparison finds significantly higher silicon on the exposed surfaces. The exposed surface oxygen concentration on all of the samples is higher and the carbon concentration is lower than on the backside surface. For all other contaminants, the exposed surface is not consistently different from the backside. Probably preflight contamination was the most significant factor for the minor contaminants. LDEF backside surfaces have probably accumulated some surface contamination on flight, but, experimentally, the LDEF-exposed surface contamination levels are generally higher for the major species, silicon and oxygen. The decrease in carbon concentration on the exposed surfaces is due to attenuation of the carbon fiber/organic matrix signals by contaminant build-up.

With the exception of the L-C and T-C, it was observed that Si contamination levels are higher on the leading edge surfaces than on the trailing edge surfaces, in spite of atomic oxygen erosion with observed crevasse development. The predominant surface species of Si on the exposed surfaces is SiO_2, which is generally accepted to be a degradation product from silicones outgassed from LDEF components such as coatings (e.g., Z306 paint) and RTV silicones. UV radiation damage could also cause such silicone degradation. It is probable that atmospheric backscatter (i.e., collisions with residual atmosphere such as atomic oxygen), resulted in enhanced deposition of silicones and other contaminants on the leading edge flight surfaces relative to the trailing edge. The exposed leading edge surface of sample B had higher silicon and oxygen concentrations than the exposed leading edge surfaces of samples A and C, which is consistent with the lower extent of erosion on B observed in the micrographs. It is not known what role the buildup of contamination layers may have had on crevasse initiation and enlargement during atomic oxygen erosion of the leading edge surfaces. The observed decrease in exposed surface carbon concentrations is due to attenuation of the organic matrix and fiber signals by the surface-deposited SiO_2. A significant fraction of the surface carbon detected may be due to contamination residues from outgassed silicones or hydrocarbons, but XPS does not differentiate

Table 2. XPS Data for LDEF Carbon Fiber/PAA Composites

			Surface Mole %, Normalized												
		Imaged?	C	O	Si	N	F	S	Cl	Cu	Zn	Ni	Sn	Na	P
L-A	Exposed	Yes	45	42	10	2		0.6		0.3					
	Exposed	No	44	44	8	1	0.4	0.5	tr	2	0.3				
	Backside	No	71	20	2	2	3	0.1	0.1	1	tr				
T-A	Exposed	No	51	36	6	2	3	tr	0.1	3	0.2		0.1		
	Backside	No	66	26	2	1	3	0.2	0.1	1					
L-B	Exposed	Yes	17	59	19	0.6	nd	0.3	0.1	2	tr	1		nd	0.3
	Backside	Yes	59	31	3	2	2	0.2	0.2	2	nd			1	nd
T-B	Exposed	Yes	45	23	4	0.9	25	0.1	0.1	1	0.1			0.1	
	Exposed	No	46	27	3	1	19	0.1	0.2	2	0.2			1	
	Backside	Yes	70	22	2	1	3	0.1	0.2	0.7	nd			0.2	nd
L-C	Exposed	Yes	61	31	3	3	0.1	0.5	nd	0.3	nd		0.4	0.3	0.6
	Backside	Yes	67	23	4	2	3	0.1	0.2	2	nd		nd	0.1	nd
T-C	Exposed	Yes	47	39	7	2	0.4	0.2	0.4	5	0.4		tr	0.1	nd
	Backside	Yes	65	24	4	1	0.3	nd	0.3	1	0.2		tr	nd	nd
Release Cloth		No	39	4	0.7		56								

tr = trace
nd = not detected in elemental scan
blank = not detected in survey scan and no elemental scan acquired

contamination from the composite surface components in this complex system. The inability to discriminate between deposited carbon contamination and the composite matrix also makes it impossible with this data to assess chemical changes induced in the composite surface by space environment exposure.

Major concentration of degraded fluorocarbon was detected on the exposed edge surface of sample T-B. At least minor concentrations were observed on all but one of the surfaces. The observed fluorine contamination levels on other LDEF surfaces analyzed by XPS, including paints, Kapton, and aluminum alloy composites, have been lower, generally < 1 mole %. It is probable that some of the carbon/organic matrix composite surfaces have high residual fluorocarbon residue from the release cloth used in their fabrication. The surface composition of a sample of release cloth is included at the bottom of Table 2.

The minor surface contaminants detected on the composite surfaces included N, S, Cl, and Cu on most of the analyzed surfaces and Zn, Ni, Sn, Na, and P on one or more surfaces. Preflight contamination is probably a major factor for these contaminants. The exposed flight surfaces were not contaminated with detectable levels of ^{7}Be as measured by XPS or EDS. The detected concentrations of ^{7}Be on other LDEF-exposed surfaces were about 1–10 parts per billion,[9] well below the detection limits of XPS and EDS.

When a comparison of surface composition data from XPS and EDS is made, it is important to recognize the significant difference in the average depth probed: this was about 10,000 Å for EDS and about 100 Å for XPS. This difference makes XPS more sensitive to outer surface contamination than EDS and less sensitive to bulk compositional changes. The detection of Cu and F on more composite surfaces by XPS than by EDS supports the hypothesis that these components are concentrated in the outer surface layers. The general trends for the major surface contaminants, Si and O, were found to be the same by XPS and EDS, with minor differences explained by the difference in depth probed by the two techniques.

IV. CONCLUSIONS

None of the composites were catastrophically damaged by nearly six years of exposure to the space environment. The trailing edge samples exhibited no physical appearance changes due to exposure. Composites on the leading edge were eroded to a depth of about 5 mils. More quantitative measurements of the erosion level were difficult because of the irregularity of the erosion process. The erosion morphology was dominated by crevasses parallel to the fibers with triangular cross sections 10 to 100 μm in depth. The location of the crevasses was not correlated with the location of surface cracks. The edges of the crevasses were well defined and penetrated through both matrix and fiber. No preferential removal of the matrix relative to the fibers was apparent along the sides in the crevasse enlargement pattern. At the present time, we do not know the mechanism for the formation of the crevasses. However, the data suggest that the carbon fibers are playing a significant role in crevasse initiation and/or enlargement, and in the overall erosion rate. No differences in erosion behavior between matrix types can be concluded from the data currently at hand.

It is difficult to predict the long-term atomic oxygen erosion morphology of composite materials from erosion data obtained on short STS missions. A better understanding of other factors that may influence erosion, such as thermal cycling and UV exposure, is necessary to improve the accuracy of these predictions.

Major on-flight contamination from silicones and hydrocarbons was observed, as evidenced by higher levels of Si and O detected on the exposed surfaces than on the backsides. Higher levels of Si and O were detected on the leading edge exposed surfaces, in spite of atomic oxygen erosion, than on the trailing edge exposed surfaces, probably due to atmospheric backscatter. The exposed leading edge surface of sample B had higher silicon and oxygen concentrations than the exposed leading edge surfaces of samples A and C, which is consistent with the lower extent of erosion on B observed in the micrographs. The role of contamination in crevasse initiation and enlargement is unknown at this time. Good agreement was seen between EDS and XPS data on major contaminants. The presence of a wide range of minor contaminants, probably due to preflight contamination, was also observed.

REFERENCES

1. Jabloner, H., U. S. Patent No. 4,070,333 (1978).

2. Whitesides, George M., and Neenan, T. X., *J. Org. Chem.* 53, 2489-2496 (1988).

3. Barry, W. T., Gaulin, C. A., and Kobayshi, R. W., "Review of Polyarylacetylene Matrices for Thin-Walled Composites," Aerospace Report SSD-TR-89-75, The Aerospace Corporation, El Segundo CA (25 September 1989); see also Katzman, H. A., "Polyarylacetylene Resin Composites," Aerospace Report SSD-TR-90-013, The Aerospace Corporation, El Segundo CA (2 April 1990).

4. Zaldivar, R. J., Rellick, G. S., and Yang, J. M., "Processing Effects on the Mechanical Behavior of Polyarylacetylene-Derived C-C," *Sampe J.*, 27, 29 (1991); see also Zaldivar, R. J., Kobayashi, R. W., Rellick, G. S., and Yang, J. M., *Carbon*, 29, 1145 (1991).

5. Hergenrother, P. M., *J. Appl. Polym. Sci.*. 18, 1779 (1974).

6. Gregory, J. C., private communication, University of Alabama, Huntsville, AL (November 1991).

7. Meshishnek, M. J., Stuckey, W. K., Evangelides, J. S., Feldman, L. A., Peterson, R. V., Arnold, G. S., and Peplinski, D R., "Effects on Advanced Materials: Results of the STS-8 EOIM Experiment," Aerospace Report SD-TR-87-34, The Aerospace Corporation, El Segundo, CA (20 July 1987)

8. Gregory, J. C., private communication, University of Alabama, Huntsville, AL (November 1991).

9. Fishman, G. J., Harmon, B. A., Gregory, J. C., Parnell, T. A., Peters, P., Phillips, G. W., King, S. E., August, R. V., Ritter, J. C., Cutchin, J. H., Haskins, P. S. McKisson, J. E., Ely, D. W., Weisenberger, A. G., Piercey, R. B., and Dybler, T., "Observation of ^{7}Be on the Surface of LDEF Spacecraft," *Nature* 349, 678 (1991).

FIGURES

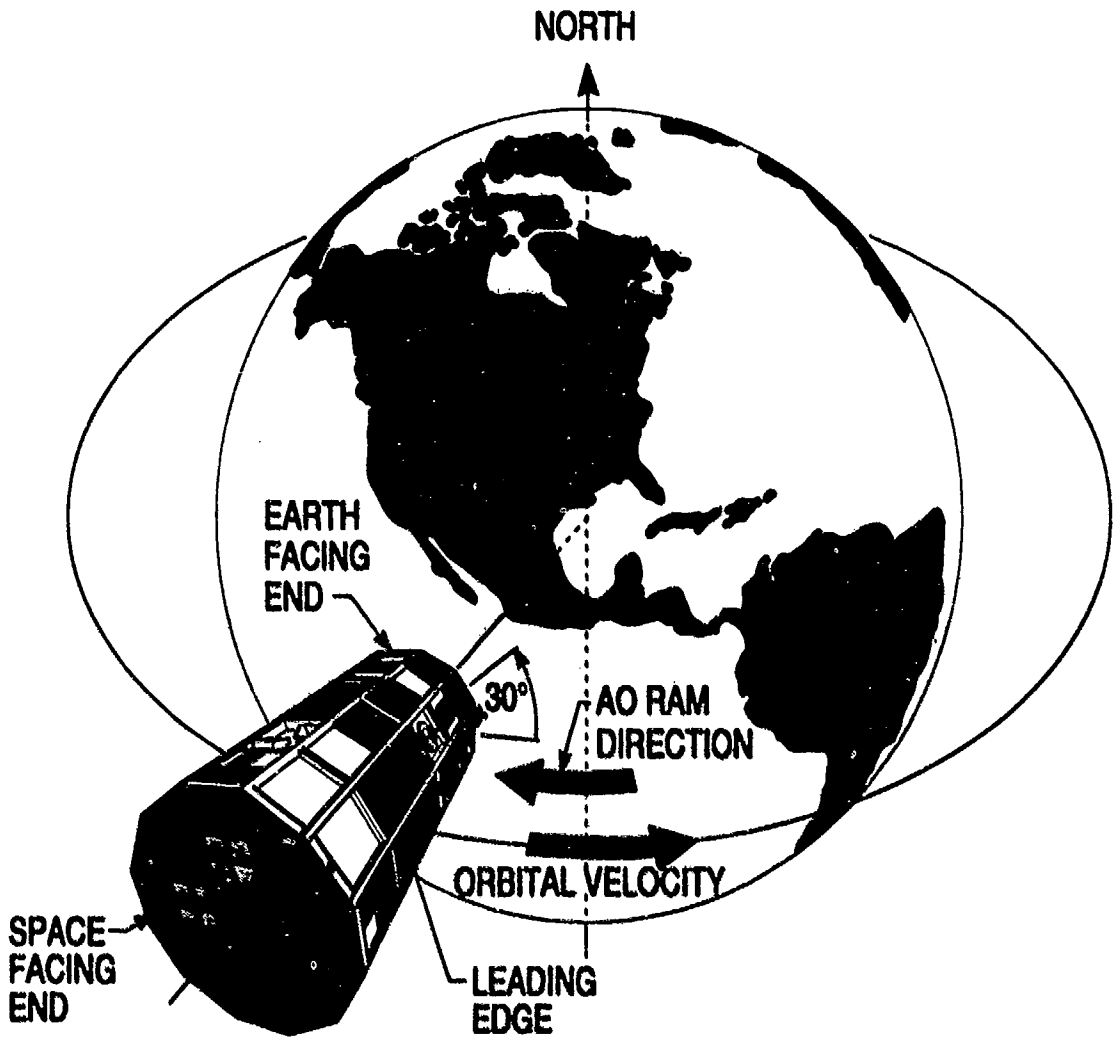

Figure 1a. Orientation of LDEF during flight (courtesy of Marshall Space Flight Center).

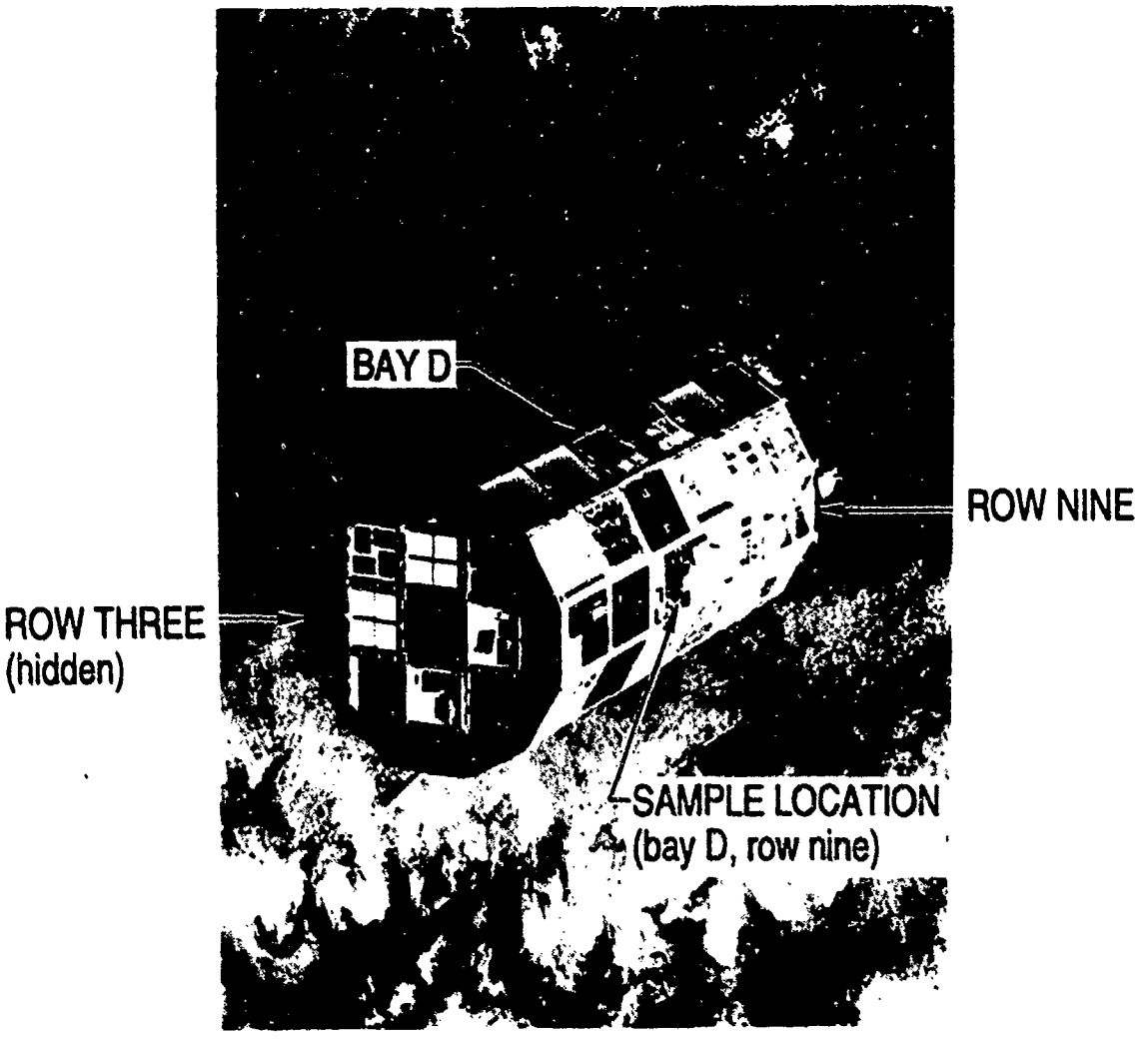

Figure 1b. On-orbit photograph of LDEF.

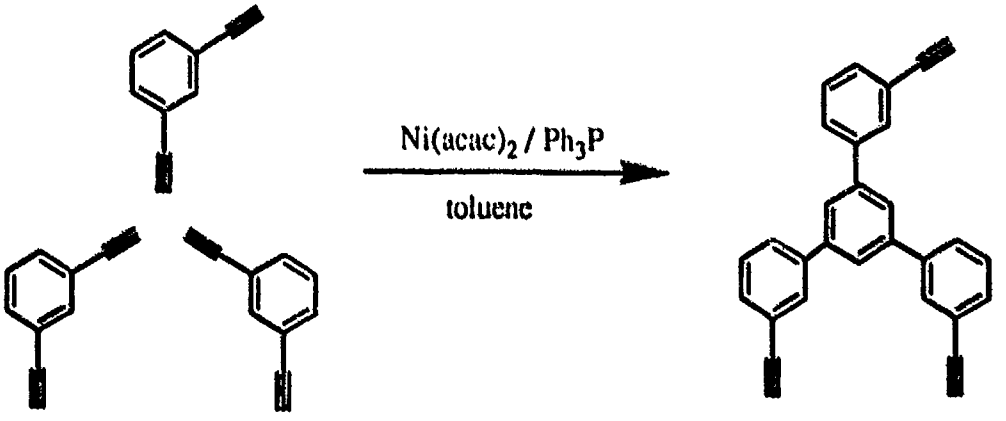

Figure 2. Cyclotrimerization reaction of diethynylbenzene (DEB).

Figure 3a. SEM micrograph (20X) of L-A surface showing exposed and masked areas.

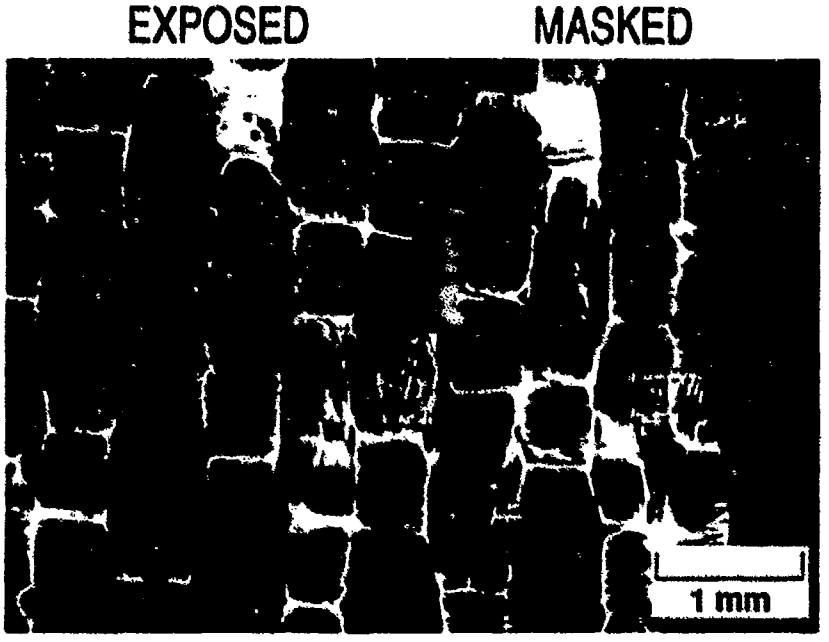

Figure 3b. SEM micrograph (20X) of T-A surface showing exposed and masked areas.

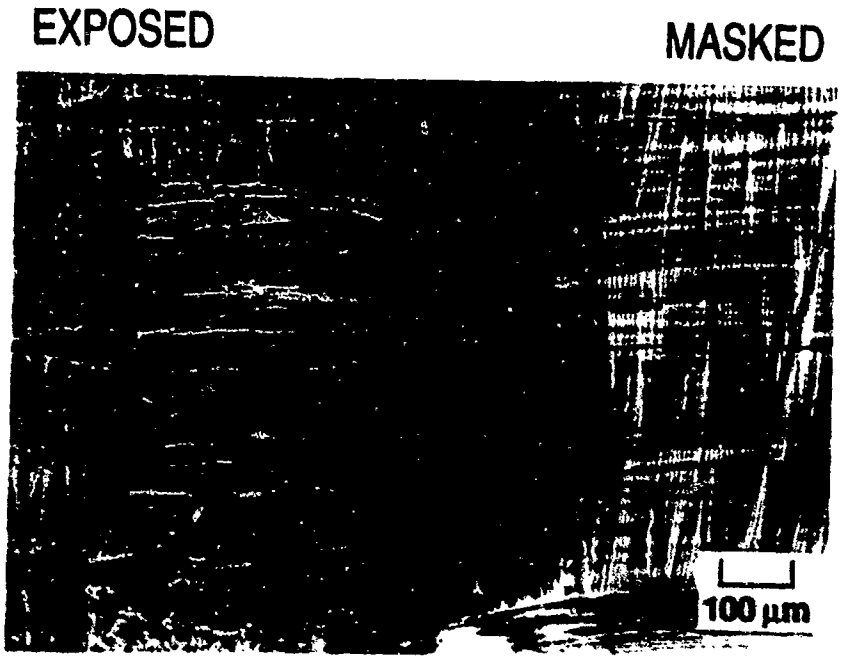

Figure 4. SEM micrograph (100X) of L-A surface showing exposed and masked areas.

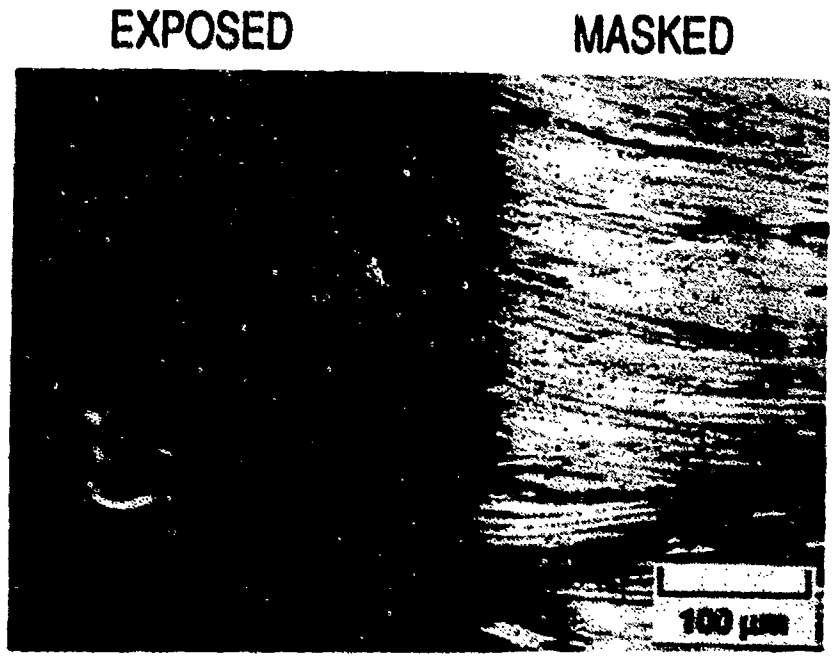

Figure 5. SEM micrograph (200X) of L-C surface showing exposed and masked areas.

Figure 6. Optical micrograph (50X) of L-A cross section.

Figure 7. Optical micrograph (50X) of L-B cross section.

Figure 8. Optical micrograph (50X) of L-C cross section.

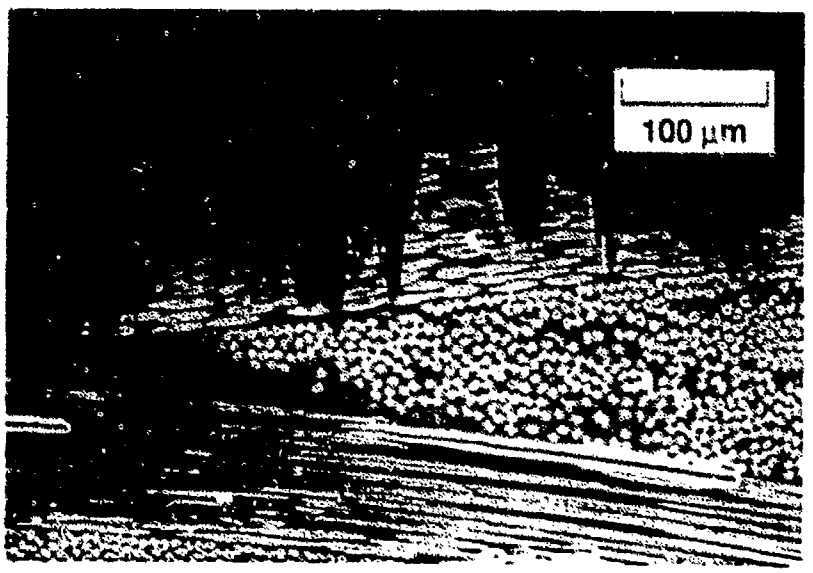

Figure 9. SEM micrograph (200X) of L-A cross section.

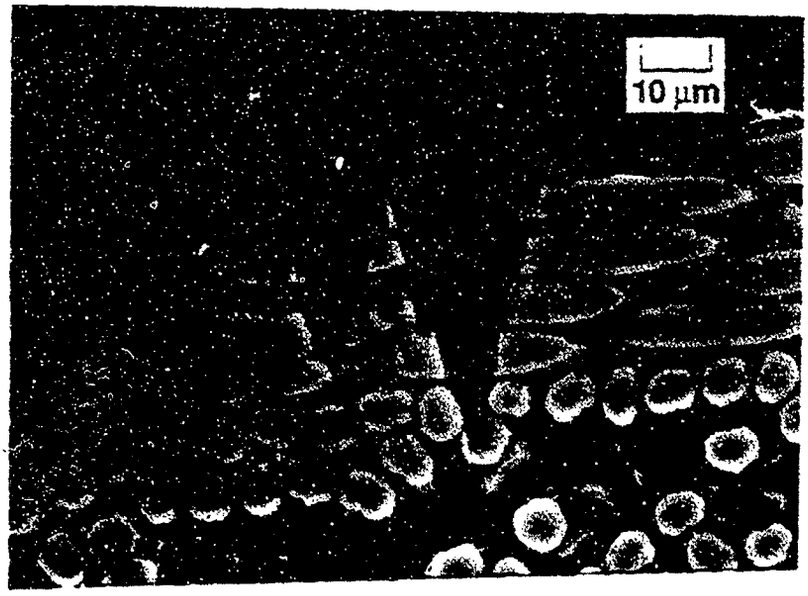

Figure 10. SEM micrograph (1000X) of L-A cross section.

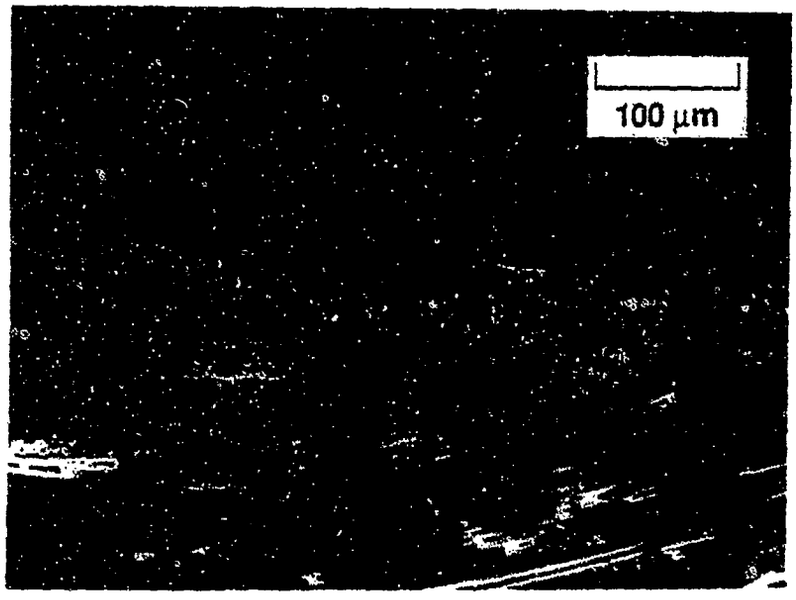

Figure 11. SEM micrograph (200X) of L-B cross section.

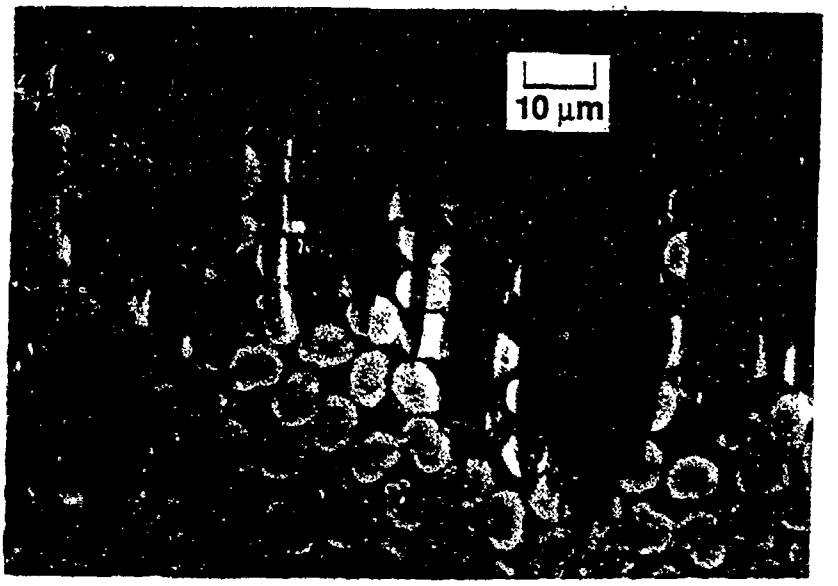

Figure 12. SEM micrograph (1000X) of L-B cross section.

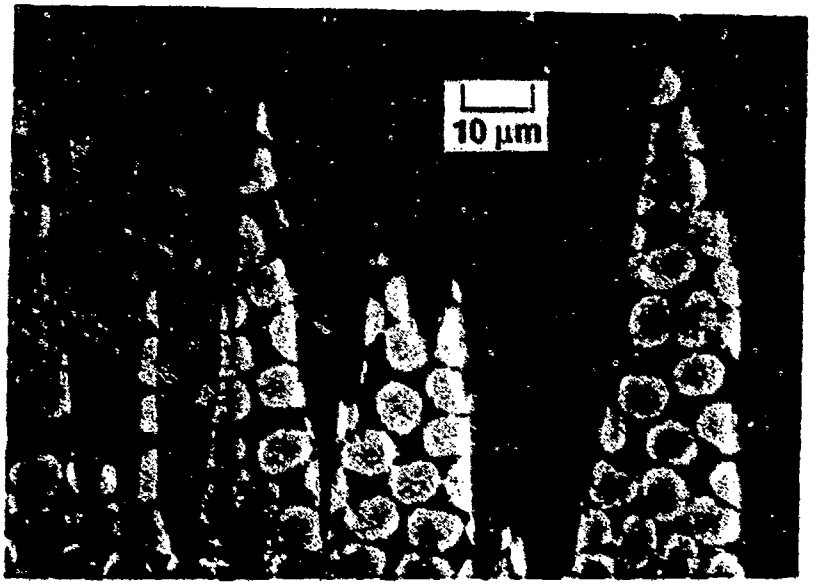

Figure 13. SEM micrograph (200X) of L-C cross section.

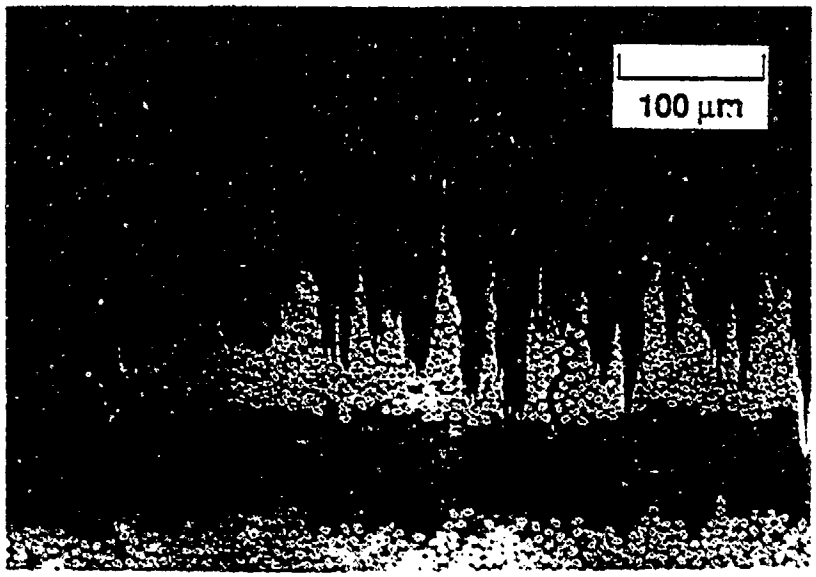

Figure 14. SEM micrograph (1000X) of L-C cross section.

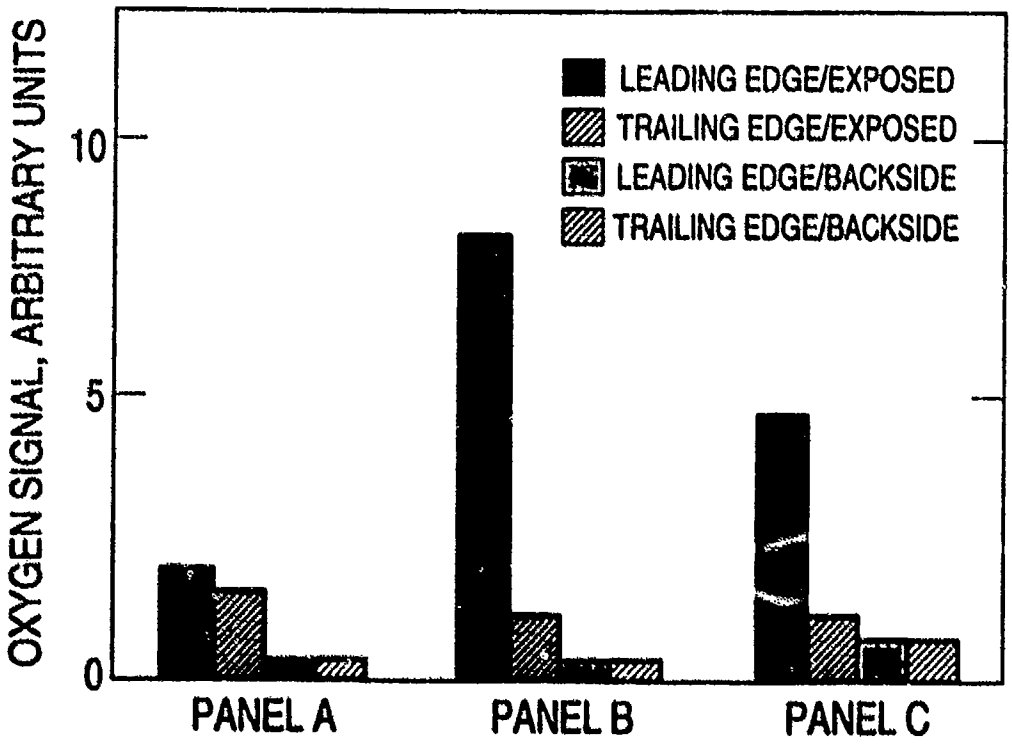

Figure 15. EDS relative oxygen signals.

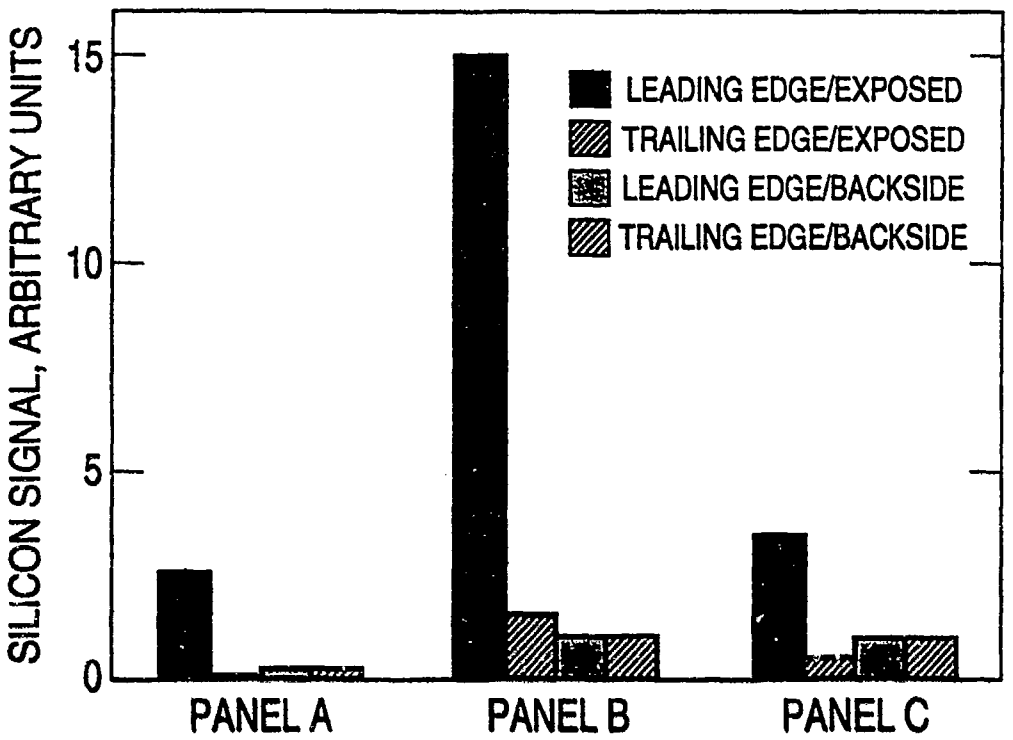

Figure 16. EDS relative silicon signals.

TECHNOLOGY OPERATIONS

The Aerospace Corporation functions as an "architect-engineer" for national security programs, specializing in advanced military space systems. The Corporation's Technology Operations supports the effective and timely development and operation of national security systems through scientific research and the application of advanced technology. Vital to the success of the Corporation is the technical staff's wide-ranging expertise and its ability to stay abreast of new technological developments and program support issues associated with rapidly evolving space systems. Contributing capabilities are provided by these individual Technology Centers:

Electronics Technology Center: Microelectronics, solid-state device physics, VLSI reliability, compound semiconductors, radiation hardening, data storage technologies, infrared detector devices and testing; electro-optics, quantum electronics, solid-state lasers, optical propagation and communications; cw and pulsed chemical laser development, optical resonators, beam control, atmospheric propagation, and laser effects and countermeasures; atomic frequency standards, applied laser spectroscopy, laser chemistry, laser optoelectronics, phase conjugation and coherent imaging, solar cell physics, battery electrochemistry, battery testing and evaluation.

Mechanics and Materials Technology Center: Evaluation and characterization of new materials: metals, alloys, ceramics, polymers and their composites, and new forms of carbon; development and analysis of thin films and deposition techniques; nondestructive evaluation, component failure analysis and reliability; fracture mechanics and stress corrosion; development and evaluation of hardened components; analysis and evaluation of materials at cryogenic and elevated temperatures; launch vehicle and reentry fluid mechanics, heat transfer and flight dynamics; chemical and electric propulsion; spacecraft structural mechanics, spacecraft survivability and vulnerability assessment; contamination, thermal and structural control; high temperature thermomechanics, gas kinetics and radiation; lubrication and surface phenomena.

Space and Environment Technology Center: Magnetospheric, auroral and cosmic ray physics, wave-particle interactions, magnetospheric plasma waves; atmospheric and ionospheric physics, density and composition of the upper atmosphere, remote sensing using atmospheric radiation; solar physics, infrared astronomy, infrared signature analysis; effects of solar activity, magnetic storms and nuclear explosions on the earth's atmosphere, ionosphere and magnetosphere; effects of electromagnetic and particulate radiations on space systems; space instrumentation; propellant chemistry, chemical dynamics, environmental chemistry, trace detection; atmospheric chemical reactions, atmospheric optics, light scattering, state-specific chemical reactions and radiative signatures of missile plumes, and sensor out-of-field-of-view rejection.